

Article

# Thermal Degradation Kinetics of Vacuum Residues in the Presence of Chrysotile Supported Ni-Ti Catalyst

Nazerke Balpanova and Murzabek Baikenov \*

Department of Chemical Technologies and Petrochemicals, Faculty of Chemistry, Karaganda Buketov University, Karaganda 100024, Kazakhstan; nazerke\_90@mail.ru

\* Correspondence: thearticle@bk.ru or murzabek\_b@mail.ru

**Abstract:** For the first time, thermal decomposition of vacuum residue and a mixture of vacuum residue with binary nanocatalysts based on leached and non-leached chrysotile with applied active metals was studied using the thermogravimetry method. It is shown that the thermokinetic parameters of decomposition of vacuum residue and its mixture with binary nanocatalyst are different. The phase composition of the binary nanocatalyst was established through X-ray phase analysis (XRD):  $(\text{Mg}_3\text{Si}_2\text{O}_5(\text{OH}))$ ,  $\text{NiO}$  and  $\text{Ti}(\text{SO}_4)_2$ . The quantitative content of elements on the chrysotile surface was determined using X-ray fluorescence analysis: (Ni (4.88%), Ti (7.29%), Si (24.93%), Mg (7.83%), Fe (0.69%) and S (3.89%)). Using atomic emission spectral analysis, the gross quantitative content of supported metals on chrysotile was determined: Ni (4.85%) and Ti (4.86%). A transmission electron microscope showed the presence of finely dispersed particles adsorbed on the surface of and possibly inside chrysotile nanotubes with sizes ranging from 5 to 70 nm. The acidity of the nanocatalyst obtained from the leached active-metal-supported chrysotile was  $267 \mu\text{mol/g}$  and the specific surface area of the nanocatalyst was  $54 \text{ m}^2/\text{g}$ . The Ozawa–Flynn–Wall (OFW) method was used to calculate the kinetic parameters of the thermal degradation of vacuum residue and the mixture of vacuum residue with nanocatalysts. Using the isoconversion method, the average values of activation energies and the pre-exponential factor were calculated:  $147.55 \text{ kJ/mol}$  and  $3.37 \cdot 10^{16} \text{ min}^{-1}$  for the initial vacuum residue;  $118.69 \text{ kJ/mol}$  and  $1.54 \cdot 10^{18} \text{ min}^{-1}$  for the mixture of vacuum residue with nanocatalyst obtained from non-leached chrysotile with applied metals;  $82.83 \text{ kJ/mol}$  and  $2.15 \cdot 10^{19} \text{ min}^{-1}$  for the mixture of vacuum residue with nanocatalyst obtained from leached chrysotile with applied metals. The kinetic parameters obtained can be used in modeling and designing the processes of thermal degradation and hydroforming of heavy hydrocarbon raw materials.

**Keywords:** vacuum residue; thermogravimetric; chrysotile; nanocatalyst; kinetics; activation energy; pre-exponential factor



**Citation:** Balpanova, N.; Baikenov, M. Thermal Degradation Kinetics of Vacuum Residues in the Presence of Chrysotile Supported Ni-Ti Catalyst. *Catalysts* **2023**, *13*, 1361. <https://doi.org/10.3390/catal13101361>

Academic Editors: Eduard Karakhanov, Aleksandr Glotov and Federica Menegazzo

Received: 21 August 2023

Revised: 25 September 2023

Accepted: 5 October 2023

Published: 11 October 2023



**Copyright:** © 2023 by the authors. Licensee MDPI, Basel, Switzerland. This article is an open access article distributed under the terms and conditions of the Creative Commons Attribution (CC BY) license (<https://creativecommons.org/licenses/by/4.0/>).

## 1. Introduction

Oil raw materials play a significant role in the global fuel and economic complex. Since the development of society, a significant amount of energy has been spent, and the efficient use of heavy oil resources, including vacuum residue, has attracted the attention of the world community. Reducing the reserves of “light” oils requires the more active use and processing of heavy hydrocarbons, such as high-viscosity oils, vacuum residue and bitumen [1–6].

Vacuum residue is a heavy fraction obtained via vacuum distillation of crude oil at a temperature of  $400\text{--}420 \text{ }^\circ\text{C}$ . Vacuum residues account for up to 40–50% of total crude oil refining, and their share is expected to grow [7]. At the oil processing plant, vacuum residue is produced in the form of a product with a cubic structure during vacuum distillation. Typically, vacuum residue is used in the production of asphalt for road surfaces [8]. It is sometimes used as fuel for combined cycle systems with integrated gasification [9]. Several attempts have also been made to use it as fuel for direct combustion in utility boilers [10,11].

The sharp recent increase in oil prices is causing serious concern about the use of vacuum residue in industry, because the price of vacuum residue is estimated to be lower than that of heavy oil. In terms of its characteristics as a fuel, vacuum residue can be described as an extremely viscous substance with a high content of carbon, sulfur, nitrogen and heavy metals [12].

Various methods are used to process heavy hydrocarbons, including thermal and catalytic cracking, hydrocracking, delayed coking and other processes. Despite the wide application of these methods in industry, they do not provide a sufficiently deep conversion of vacuum residues and have several problems, the most significant of which is associated with a high content of high-molecular-weight components, such as asphaltenes. Asphaltenes are present in oil and residual oil fractions as solid aggregates and are a dispersed phase in which the sedimentation process is difficult due to the presence of solvate resin shells and polar heteroatomic contained in the feedstock. In addition, as the viscosity of the produced oil increases, the content of asphaltenes in it also increases [13,14].

A large number of studies conducted in the literature [15–19] are devoted to the study of the composition, properties and structure of heavy oil residues. However, due to the complexity of their structure and the ability to form large agglomerates, the exact molecular weight of heavy oil residues is difficult to determine. In this regard, the problem of establishing reliable, experimentally confirmed mechanisms for the conversion of vacuum residue molecules in thermal processes is still unresolved. An important aspect of understanding the thermal stability of petroleum residues is calculating the kinetic patterns of their transformations in the process of thermal cracking.

The study of the kinetics of the fuel pyrolysis process contributes to the development of technologies aimed at improving the design of reactors and more efficient use of heavy oils [20]. Methods such as model and model-free approaches are used in the calculation of kinetic parameters. Model-free methods (for example, the Friedman method, the Ozawa–Flynn–Wall method and the Kissinger–Akahira–Sunose method) allow for determining the activation energy without involving a reaction model, which reduces the errors caused by an incorrect determination of the mechanism [21]. As the most versatile of the model-free approaches, the Friedman method provides a more reliable definition of activation energy due to its widespread use for accurate processing of specific data and its ability to avoid the complex mathematical problem associated with the temperature integral [22,23]. However, in practical kinetic analysis, simple, computationally effective integration methods (for example, the Ozawa–Flynn–Wall method) are more often used [22].

The literature presents the regularities of vacuum residue thermal degradation in the presence of various heterogeneous catalysts, where group VI and VIII metals (Mo, Ni, Fe, Co) supported on  $\text{Al}_2\text{O}_3$  [24–27] and zirconium oxide deposited on red sludge [28,29] are used as an active component. Nevertheless, it is necessary to emphasize the important function of the acid component in the catalyst; it is active in cracking and isomerization processes, which are characteristic features of zeolites [30,31]. Chrysotile asbestos also has acidic properties. Asbestos nanotubes, which are a natural product of rock formation, have unique mechanical properties [32]. Nanotubes represented by chrysotile have a surface structure, which makes them the most suitable objects for physical sorption. Due to the developed surface (with a specific surface area of  $20 \text{ m}^2/\text{g}$ ) and the packaging of nanotubes with hydrophilic properties, chrysotile has a high sorption ability. A distinctive feature of nanotubes compared to other sorbent materials is their high sorption [33]. Researchers working with carbon nanotubes [34,35] distinguish their peculiarity: when the sorbed substance is captured inside the tube, its transformation occurs, and the sorbed substance is held in the channel while maintaining the sorption ability in the interval between the tubes. It should be noted that for the sorbate, ingress into the channel or annulus is energetically advantageous, which ensures a stable state of the substance after sorption. This property is of interest in the development of new cheap nanocatalysts [32].

The purpose of this work is to study the kinetics of thermal degradation of vacuum residue and its mixture with nanocatalysts at different rates of heating.

## 2. Results

### 2.1. Physicochemical Characteristics of the Nanocatalyst

The X-ray diffraction (XRD) of the original chrysotile and the obtained nanocatalyst samples was performed on a Dron-4-07 powder X-ray diffractometer at 30 kV/20 mA using a cobalt (Co) anode tube at a scanning rate of 4 °/min.

According to XRD, the original chrysotile had the following composition: 7.3; 3.64; 2.53; 1.53 Å-Mg<sub>3</sub>Si<sub>2</sub>O<sub>5</sub> (OH)<sub>4</sub> (Figure 1a). XRD of the obtained binary nanocatalyst based on leached chrysotile with applied active metals showed the presence of an intensive reflex 7.3; 3.64; 2.53; 1.53 Å-Mg<sub>3</sub>Si<sub>2</sub>O<sub>5</sub> (OH), reflex 2.41; 2.09; 1.48; 1.26 Å-NiO and 3.54-Ti (SO<sub>4</sub>)<sub>2</sub> (Figure 1b).

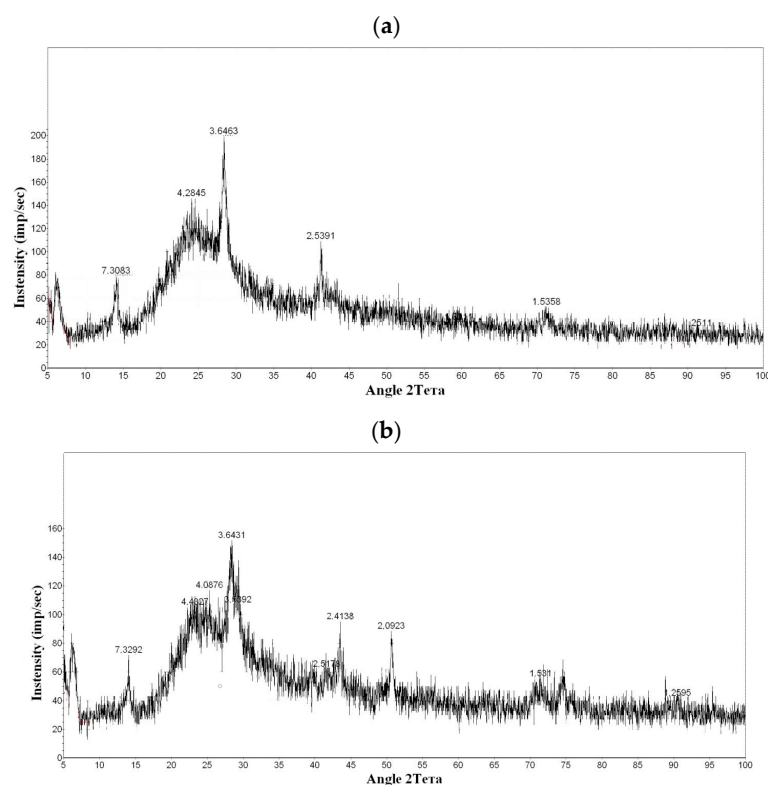


**Figure 1.** X-ray diffraction (XRD): (a) original chrysotile; (b) nanocatalyst based on leached chrysotile with applied active metals.

The quantitative contents of the elements on the chrysotile surface were determined via X-ray fluorescence analysis on a 30 kV X-ray tube FOKUS-2M spectrometer.

According to the results of X-ray fluorescence analysis of the nanocatalyst, the quantitative contents of elements were determined: Ni (4.88%), Ti (7.29%), Si (24.93%), (7.83%), Fe (0.69%) and S (3.89%).

The gross contents of nickel and titanium in the nanocatalyst are shown in Table 1. The quantitative contents of nickel and titanium were obtained using a Profile Plus atomic emission spectrometer at 21 °C and an atmospheric pressure of 727 mm Hg.

**Table 1.** Gross nickel and titanium contents in the nanocatalyst.

Name	Analyte	Unit of Measure	Content of Component
Nanocatalyst	Nickel (Ni)	%	4.85
	Titanium (Ti)	%	4.86

The presence of finely dispersed nickel and titanium particles on the surface and possibly inside the chrysotile tubes was evaluated using a Joel Jem-1400Plus transmission

electron microscope (Freising, Germany) with an accelerating voltage of 120 kV. According to the micrograph (Figure 2), there were metal particles with sizes from 5 to 70 nm on the surface and inside the chrysotile nanotubes.

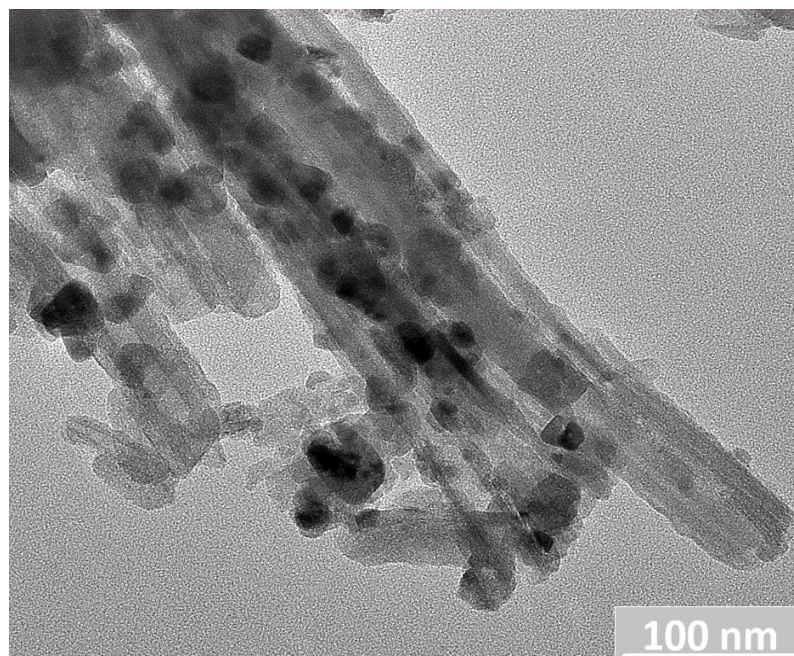


**Figure 2.** Micrograph of a chrysotile-based nanocatalyst with active metals applied.

To confirm the presence of acidic properties of non-leached and leached metal-supported chrysotile, a thermally programmed desorption (TPD) analysis of ammonia was performed. Based on the optimal ammonia desorption rate on the temperature curve, a clear maximum was observed at 110 °C with an acid center concentration of 67  $\mu\text{mol/g}$  for non-leached chrysotile with applied active metals, and 200 °C with an acid center concentration of 267  $\mu\text{mol/g}$  for leached chrysotile, respectively.

The specific surface areas of the starting chrysotile and the leached active-metal-supported chrysotile were investigated through low-temperature nitrogen adsorption at 77 K. Measurements were carried out on an automated volumetric installation Digisorb-2600 (Micromerics, USA). Each sample was pre-trained under a vacuum at 350 °C for 5 h.

In addition, a standard method for processing isotherms of polymolecular adsorption was used—the Brunauer–Emmett–Teller method (BET). At the same time, the device software was also involved. The BET analysis yielded surface areas of the original chrysotile and nanocatalyst derived from the leached metal-added chrysotile of 39.4 and 54  $\text{m}^2/\text{g}$ , respectively.

Thermogravimetric curves were constructed to assess the effect of the obtained nanocatalysts on vacuum residue thermal degradation (Figure 3a–c).

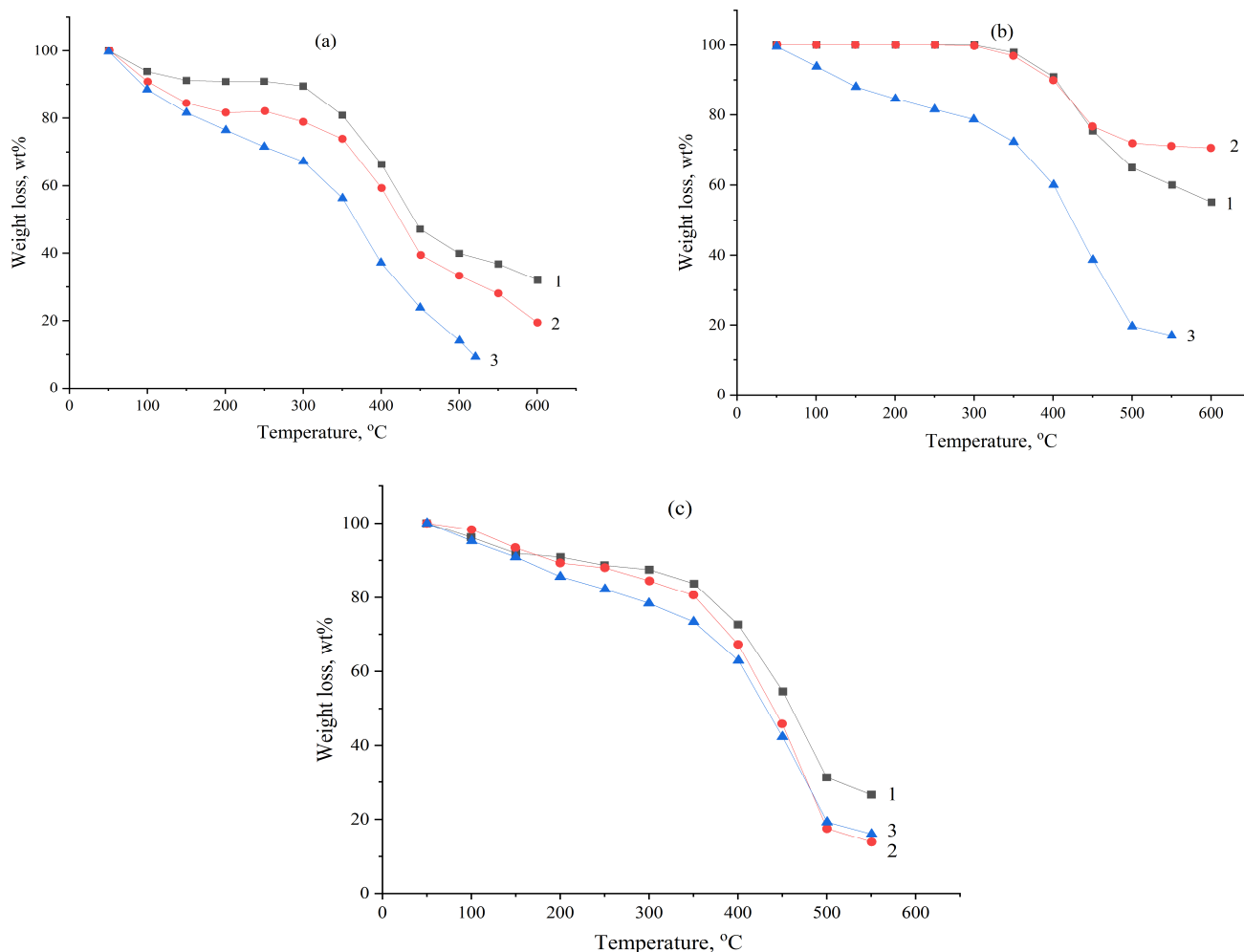


**Figure 3.** Dependence of sample weight loss on temperature: (a) at heating rate of 10 °C/min; (b) at a heating rate of 20 °C/min; (c) at heating rate of 30 °C/min; 1—vacuum residue (sample 1), 2—mixture of vacuum residue with nanocatalyst, obtained from non-leached chrysotile with applied active metals (sample 2), 3—mixture of vacuum residue with nanocatalyst, obtained from leached chrysotile with applied active metals (sample 3).

### 2.2. Thermal Decomposition Kinetics of Vacuum Residue and Its Mixture with Nanocatalyst

The determination of activation energy is based on the generalized expression (1) for the rate of decomposition of the vacuum residue and its mixture with nanocatalysts.

The activation energy and the coefficient of the pre-exponential factor of the rate of decomposition of the vacuum residue and its mixture with nanocatalysts were calculated using Equation (4) of the Ozawa–Flynn–Wall method.

The results of Equation (4) are arranged in straight lines on the inverse temperature  $\ln\beta$  plots. The plots are valid for various temperature measurements carried out in the process of thermal decomposition of the tar and its mixture with nanocatalysts at heating rates (10, 20 and 30 °C/min) and for different degrees of conversion of  $\alpha$  samples. The result obtained makes it possible to calculate the activation energy value from the tangent of the inclination angle (Figure 4a–c).

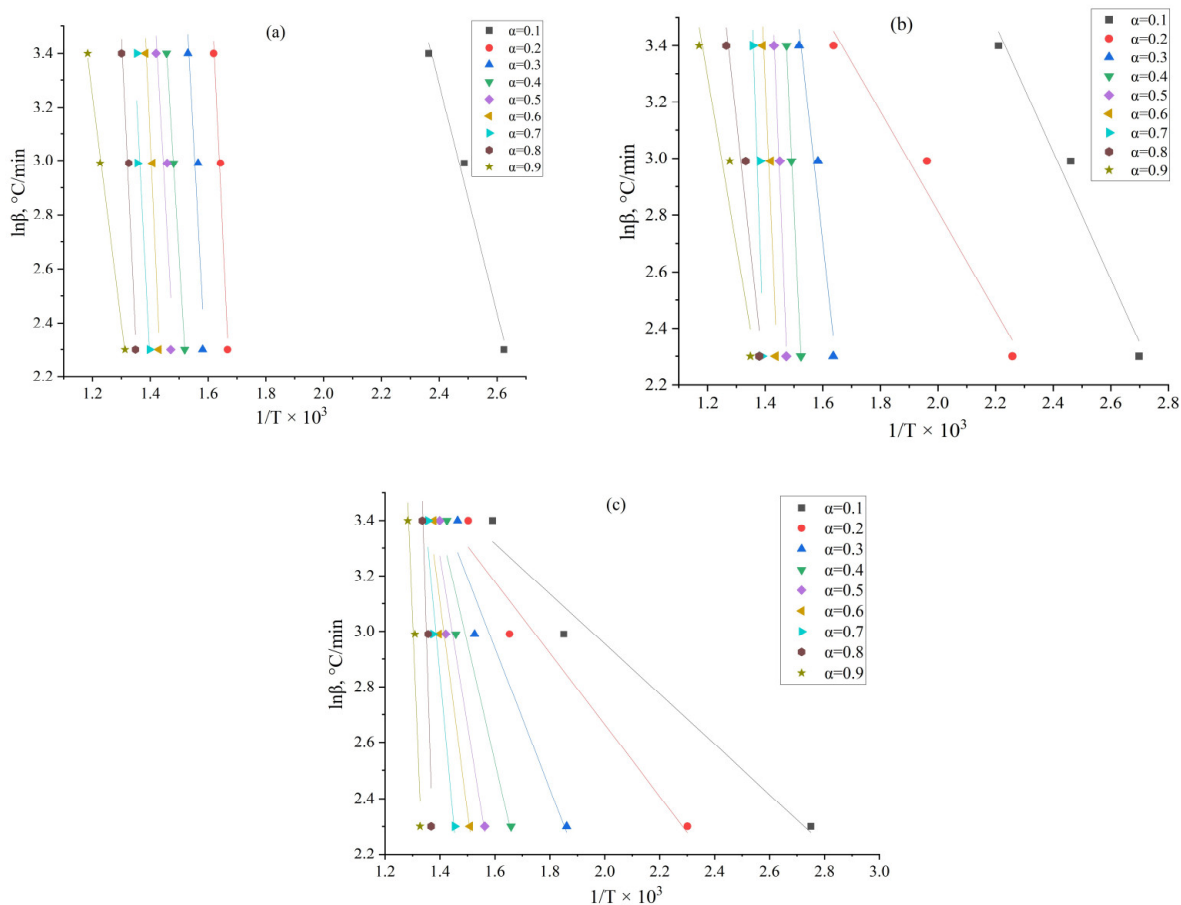


**Figure 4.** Arrhenius dependencies based on the OFW method: (a) sample 1; (b) sample 2; (c) sample 3.

Using the  $\ln\beta$ - $1/T$  plot (Figure 4a–c), the activation energy and the pre-exponential factor of the rate of decomposition of the vacuum residue and its mixture with nanocatalysts were calculated. The  $\ln\beta$ - $1/T$  plot shows straight line plots known as isoconversion lines, and the slope tangent of these lines is directly related to the activation energy (see Figure 4a–c). The results of the activation energy calculation for thermal decomposition of vacuum residue and its mixture with nanocatalysts performed using the OFW method are presented in Table 2 and Figure 5a–c.

**Table 2.** Kinetic parameters of vacuum residue thermal degradation and mixture of vacuum residue with nanocatalysts obtained using OFW method.

$\alpha$ .	Sample 1		Sample 2		Sample 3	
	$E_{a,r}$ kJ/mol	$A, \text{min}^{-1}$	$E_{a,r}$ kJ/mol	$A, \text{min}^{-1}$	$E_{a,r}$ kJ/mol	$A, \text{min}^{-1}$
0.1	35.26	$7.04 \cdot 10^5$	18.70	$4.54 \cdot 10^3$	7.50	$1.16 \cdot 10^2$
0.2	188.89	$2.97 \cdot 10^{17}$	14.66	$5.66 \cdot 10^2$	10.69	$1.88 \cdot 10^2$
0.3	166.04	$6.01 \cdot 10^{14}$	76.11	$3.43 \cdot 10^7$	21.06	$1.10 \cdot 10^3$
0.4	145.64	$3.62 \cdot 10^{12}$	180.99	$2.55 \cdot 10^{15}$	35.40	$1.14 \cdot 10^4$
0.5	158.76	$1.92 \cdot 10^{13}$	212.97	$2.55 \cdot 10^{17}$	50.30	$1.25 \cdot 10^5$
0.6	197.64	$6.14 \cdot 10^{15}$	193.23	$3.55 \cdot 10^{15}$	62.70	$8.61 \cdot 10^5$
0.7	176.05	$6.97 \cdot 10^{13}$	248.86	$1.36 \cdot 10^{19}$	87.90	$4.60 \cdot 10^7$
0.8	189.57	$2.40 \cdot 10^{14}$	77.80	$4.40 \cdot 10^6$	269.20	$1.94 \cdot 10^{20}$
0.9	70.10	$6.33 \cdot 10^5$	44.86	$1.77 \cdot 10^4$	200.70	$8.98 \cdot 10^{14}$
Mean value	147.55	$3.37 \cdot 10^{16}$	118.69	$1.54 \cdot 10^{18}$	82.83	$2.15 \cdot 10^{19}$
Correlation coefficient, $R^2$	0.9797		0.9289		0.988	

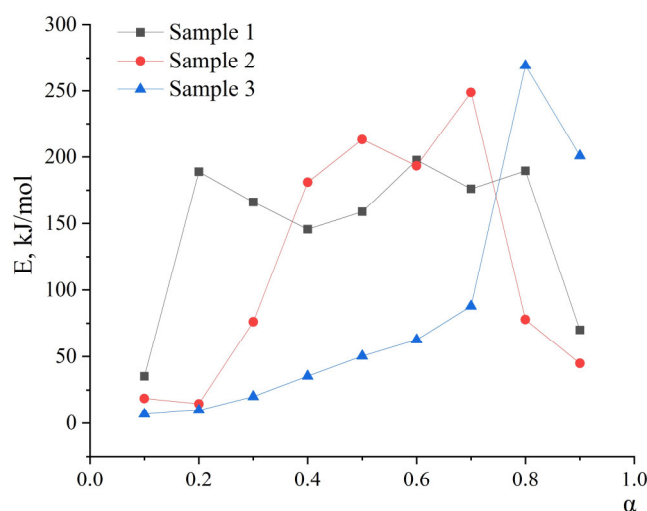


**Figure 5.** Dependence of activation energy on the degree of the conversion of samples.

The results of the activation energy calculation for thermal decomposition of the vacuum residue and its mixture in the presence of nanocatalysts using the OFW method demonstrate high correlation coefficient ( $R^2$ ) values. The high degree of consistency between the experimental data presented in Table 2 and those obtained using the OFW method indicates the usefulness of the proposed model-free method for evaluating the kinetics of thermal decomposition of vacuum residue and its mixture with nanocatalysts under selected conditions.

Perhaps the change in activation energy depending on the degree of  $\alpha$  conversion shows the complexity of the thermal degradation reaction of the original tar and the mixture of tar with nanocatalysts, which involve many parallel reactions (Figure 5a–c).

### 3. Discussion

Figure 3a shows that at a heating rate of 10 °C/min, the conversion was 60 wt% for sample 1 (in the temperature range from 270 to 500 °C); 69 wt% for sample 2 (in the temperature range from 220 to 500 °C); and 86 wt% for sample 3 (in temperature range from 50 to 500 °C). At a heating rate of 20 °C/min, the conversion was 35% for sample 1 (in the temperature range from 300 to 500 °C); 28 wt% for sample 2 (in the temperature range from 270 to 500 °C); and 80 wt% for sample 3 (in the temperature range from 50 to 500 °C) (Figure 3b). For a heating rate of 30 °C/min, the conversion was 69 wt% for sample 1 (in the temperature range from 180 to 500 °C); 82 wt% for sample 2 (in the temperature range from 80 to 500 °C); and 81 wt% for sample 3 (in the temperature range from 50 to 500 °C) (Figure 3c). Comparison of the TG curves in Figure 3a–c of the thermal degradation of sample 1 with samples 2 and 3 shows a shift in the mass loss curve of the vacuum residue mixture with binary nanocatalysts to the low temperature region, which confirms the positive effect of the nanocatalysts.

Thus, a binary nanocatalyst based on leached chrysotile with supported active metals (nickel and titanium) showed high activity. The conversion degree of sample 3 at a heating rate of 10 °C/min was 86 wt.% at 500 °C, whereas the conversion rate of sample 1 at the same temperature was 60 wt.% and of sample 2 was 69 wt.%. This confirmed our earlier conclusions in [36] on the thermal decomposition of a mixture of low-temperature coal vacuum residue resin with a chrysotile-based catalyst. We have found that the rate of vacuum residue thermal degradation depends on the qualitative composition added to the nanocatalyst.

The study of TG curves (Figure 3a–c) and the dependence of activation energy on the degree of  $\alpha$  conversion (Figure 5) allowed us to distinguish the following patterns: with an increase in the conversion degree of sample 1 from 0.1 to 0.8, the activation energy increased from 35.3 to 189.6 kJ/mol (Table 2). Apparently, this is due to the thermal

decomposition at the initial stage of the weakest aliphatic bonds in oils and resins, and the further decomposition of the vacuum residue with the release of volatile substances as the temperature increases proceeds with an increasingly high energy activation. That is, thermally more stable molecular fragments of heavy resins and asphaltenes are involved in the destruction process. This is consistent with data from other studies [37]. In the case of sample 2, at the initial stage, with an increase in the conversion degree from 0.1 to 0.3, the activation energy values showed lower values from 18.7 to 76.1 kJ/mol compared to sample 1 (Table 2), which showed the positive effect of the nanocatalyst on the vacuum residue thermal decomposition process. A further increase in the conversion degree from 0.4 to 0.7 led to an increase in activation energy values from 181 to 249 kJ/mol; apparently this is due to the effect of the organic-mineral structure, which is formed as a result of thermal destruction of the vacuum residue with a nanocatalyst (non-leached chrysotile with applied active metals) or the thermal decomposition of the vacuum residue. It should be noted that non-leached chrysotile contains alkali and alkaline earth metals (Na, Ca and Mg) that inhibit the thermal decomposition process. It is possible that the increase in activation energy values is also due to the breakdown of the strongest C–C bonds of side chains and hydrocarbon bridges. With respect to samples 1 and 2, it can be seen that the degradation rate of sample 3 shows a strong effect of a leached chrysotile nanocatalyst with active metals added (Figure 5). With an increase in conversion from 0.1 to 0.7, a gradual increase in activation energy is observed from 7.50 to 87.90 kJ/mol, which indicates that the leached chrysotile-supported nanocatalyst increases the decomposition rate compared to samples 1 and 2, leads to a sharp decrease in activation energy values and increases the preexponential factor (Table 2). The high activity of the prepared nanocatalyst may be due to its high acidity, with an acid center concentration of 267  $\mu\text{mol/g}$ . With a further increase in the degree of conversion ( $\alpha$ ) above 0.7, the value of the activation energy increases sharply, which is associated with a delayed rate of mass loss. The use of the OFW method shows a high correlation coefficient for experimental data of the vacuum residue thermal decomposition.

Thus, it has been shown that the value of the activation energy of the vacuum residue thermal degradation and of its mixture with nanocatalysts depends on the degree of its  $\alpha$  conversion. Nanocatalysts have been found to initiate the rate of vacuum residue thermal degradation. It has been shown that leached chrysotile with supported active metals significantly increases the conversion of vacuum residue and accelerates the degradation reaction of the transition from diffusion to the kinetic region. We have found that an increase in activation energy indicates the need for a greater energy contribution to the reaction. Weak bonds, such as heteroatomic chemical bonds within a chain, are expected to be the first to break in a region with low activation energy. The side chains or random reactions requiring higher energy then break, and finally, the main chains break as the reaction completes.

#### 4. Materials and Methods

The vacuum residue of Pavlodar petrochemical plant of the Republic of Kazakhstan was used as the research object. Elemental composition of heavy petroleum residues (HPR): C—72.5%, H—11.8%, N—0.9%, S—2.6%, O—2.3%, A—1.64%. The boiling point of HPR is 550 °C, and the kinematic viscosity of HPR at 70 °C is  $262 \times 10^{-6} \text{ m}^2/\text{s}$ . HPR density is  $1.000 \text{ kg/m}^3$ . Asphaltene content is 9.8%, resins—12.5% and oils—78.2%

Non-leached and leached chrysotile were used for the nanocatalyst carrier. The chrysotile was leached with a 20% hydrochloric acid solution. The application of active metals such as titanium and nickel to the surface and inside of chrysotile nanotubes was carried out via a moisture impregnation method using aqueous solutions of nickel ( $\text{NiNO}_3 \cdot 6\text{H}_2\text{O}$ ) and titanium ( $\text{TiOSO}_4 \cdot 2\text{H}_2\text{O}$ ) salts. The resulting samples were dried at 105 °C and cooled to room temperature. The samples were then aged in a muffle furnace at 550 °C for 2 h. The amount of nanocatalyst added to the vacuum residue was 1 wt%.

Experiments to study the kinetic patterns of thermal degradation of vacuum residue and its mixture with nanocatalysts were carried out on a LabsysEvoSetaram thermal analyzer (Caluire, France) at linear heating rates ( $\beta$ ) of 10, 20 and 30 °C/min in non-isothermal mode. For each of the destructive experimental sessions with vacuum residue and its mixture with nanocatalysts, we took about 10 mg of the sample and placed it in a crucible that was made of alumina and connected to a weight system. The temperature of the sample was monitored using a thermocouple. The thermal decomposition process was carried out using a flow of nitrogen gas at a constant flow rate of 100 mL/min. The samples were heated from room temperature to 700 °C at different constant heating rates ( $\beta$ ) of 10, 20 and 30 °C/min. During the experiment, changes in sample weight and furnace temperature were recorded. The volatile components formed during the thermal decomposition process were removed via nitrogen pumping, while the non-volatile products remained as solids on the alumina crucible. All thermal analysis tests were performed two or three times at each heating rate, and the results showed a high degree of repeatability.

#### Non-Isothermal Kinetics Method

The rate of loss of the vacuum residue mass and its mixture with nanocatalysts can be described by the kinetic equation of the form [38]:

$$\frac{d\alpha}{dT} = \frac{A}{\beta} e^{\left(\frac{-E}{RT}\right)} f(\alpha), \quad (1)$$

where  $\alpha$  is the degree of conversion of the feedstock;  $\beta$  is the linear rate of sample heating, °C/min;  $A$  is the pre-exponential factor,  $c^{-1}$ ;  $T$  is the absolute temperature, K;  $E$  is the activation energy, kJ/mol;  $R$  is the universal gas constant, J/mol, K;  $f(\alpha)$  is the mathematical model of a dimensionless kinetic function, depending on the type and mechanism of reaction. The  $\alpha$  value in Equation (1) is the relative degree of the conversion of the vacuum residue and its mixture with nanocatalysts, defined as  $\alpha = \frac{m_s - m}{m_s - m_f}$ , where  $m_s$  and  $m_f$  are the initial and final mass of the substance and  $m$  is the mass of the substance at the measurement point.

According to the principles of the Ozawa–Flynn–Wall method for non-isothermal kinetics described in [39], by integrating Equation (1) and then applying a logarithm, Equation (2) can be obtained:

$$\ln G(\alpha) = \ln\left(\frac{AE}{R}\right) - \ln\beta + \ln p(z). \quad (2)$$

For a first-order reaction,  $G(\alpha)$  is

$$\int_0^{\alpha} \frac{d\alpha}{f(\alpha)} = \int_0^{\alpha} \frac{d\alpha}{1-\alpha} = -\ln(1-\alpha); \quad (3)$$

$$p(z) = \frac{e^{-z}}{z} - \int_{-\infty}^z \frac{e^{-z}}{z} dz; z = \frac{E}{RT} \quad (4)$$

The application of the Doyle approximation [40] allows us to derive Equation (3), which can be used as a substitution for expression (2):

$$\ln p(z) = -5.3305 - 1.052z. \quad (5)$$

The Ozawa–Flynn–Wall method is based on the assumption that the reaction rate at a constant  $\alpha$  value depends only on temperature. The following equation [41,42] is used in the analysis of non-isothermal kinetics:

$$\ln \beta = \ln \left[ \frac{AE}{RG(\alpha)} \right] - 5.331 - 1.052 \frac{E}{RT} \quad (6)$$

Substitutions (2) and (3) result in the equation of the OFW (4) for calculating the temperature-inverse ratio of the heating rate of the vacuum residue and its mixture with the nanocatalysts. Activation energy and pre-exponential factor were calculated. Using the Ozawa–Flynn–Wall method, we evaluated the kinetic parameters of the process of thermal decomposition of vacuum residue and a mixture of vacuum residue with nanocatalysts under non-isothermal conditions. Analysis of the literature sources [22,41] showed that the Ozawa–Flynn–Wall method is more effective than the known methods for determining kinetic parameters of heavy hydrocarbon raw materials destruction since simple computationally effective integration methods are used. Therefore, we used the Ozawa–Flynn–Wall method to determine the kinetic parameters of thermal degradation of vacuum residue and its mixture with nanocatalysts.

## 5. Conclusions

1. For the first time, an analysis of the physicochemical characteristics of binary nanocatalysts was carried out. Using X-ray phase analysis, the phase structures of the original chrysotile and nanocatalyst were determined. Using X-ray fluorescence analysis, the quantitative contents of elements on the surface of the nanocatalyst were determined. TEM microphotographs showed the distribution of nickel and titanium particles in sizes from 5 to 70 nm. The presence of acidic properties was confirmed in a nanocatalyst prepared from leached chrysotile with supported metals. Using the BET method, the specific surfaces of the samples of the starting chrysotile and nanocatalyst were established.
2. Thermogravimetric mass loss curves of vacuum residue and a mixture of vacuum residue and binary nanocatalysts were obtained for each sample. The curves showed the maximum weight loss of a sample consisting of a mixture of vacuum residue and a nanocatalyst obtained from leached metal-supported chrysotile. High weight loss appeared to be associated with high acidity of the prepared nanocatalyst.
3. The study using the isoconversion of the Ozawa–Flynn–Wall method revealed that the values of activation energy of sample 1 with an increase in the conversion degree ( $\alpha$ ) increased from 0.1 to 0.8. For sample 2, there was a decrease in activation energy at a  $\alpha$  conversion of 0.1 to 0.3 compared to sample 1. Non-leached chrysotile, which was a carrier for the nanocatalyst, showed a relatively high rate of thermal decomposition of the vacuum residue. With an increase in the conversion degree from 0.4 to 0.7, the activation energy was increased to 249 kJ/mol at a conversion degree of 70%. It is important to take into account the complex chemical composition of the vacuum residue and the change in the activation energy of thermal decomposition at different stages of the process. These changes may be due to parallel reactions with different activation energies. For sample 3, there was a gradual increase in activation energy values with an increase in  $\alpha$  conversion from 0.1 to 0.7. Low activation energy values were associated with the high acidity of the prepared nanocatalyst. The maximum mass loss in sample 3 was due to the activity of the binary nanocatalyst, which was confirmed by the average activation energy (82.83 kJ/mol) and the pre-exponential factor ( $2.15 \cdot 10^{19} \text{ min}^{-1}$ ).
4. The conducted studies were aimed at determining the kinetic characteristics of the processes of thermal decomposition of vacuum residue and a mixture of vacuum residue with binary nanocatalysts, and the results can be used in the creation of models for the analysis of thermal destruction, the catalytic hydrogenation of fuel assemblies

and the development of reactor designs for the processing of fuel assemblies (oil residues, oil sludge and high-viscosity oils).

**Author Contributions:** Conceptualization, N.B. and M.B.; methodology, N.B. and M.B.; software, N.B. and M.B.; validation, N.B. and M.B.; formal analysis, N.B. and M.B.; investigation, N.B. and M.B.; resources, N.B. and M.B.; data curation, N.B. and M.B.; writing—original draft preparation, N.B. and M.B.; writing—review and editing, N.B. and M.B.; visualization, N.B. and M.B.; supervision, N.B. and M.B.; project administration, N.B. and M.B.; funding acquisition, N.B. and M.B. All authors have read and agreed to the published version of the manuscript.

**Funding:** This work was carried out with the financial support of the Ministry of Science and Higher Education of the Republic of Kazakhstan, project No. 0122RK00092 “Nanocatalytic System for the Hydrotreatment of Heavy Hydrocarbons,” agreement No. 143/ZhG-1-22-24 of 21.06.2022.

**Data Availability Statement:** Not applicable.

**Acknowledgments:** We would like to acknowledge Yelena Senina for her support of this work.

**Conflicts of Interest:** The authors declare no conflict of interest.

## References

1. Visaliev, M.Y.; Shpirt, M.Y.; Kadiev, K.M.; Dvorkin, V.I.; Magomadov, E.E.; Khadzhiev, S.N. Integrated conversion of extra-heavy crude oil and petroleum residue with the recovery of vanadium, nickel, and molybdenum. *Solid Fuel Chem.* **2012**, *46*, 100–107. [[CrossRef](#)]
2. Timoshkina, V.V.; Zurnina, A.A.; Solmanov, P.S.; Maximov, N.M.; Pimerzin, A.A. Study of Thermocatalytic Destruction of Deasphalted Oil Heavy Petroleum Feedstock in the Presence of Catalysts Formed from Oil-Soluble Precursors. *Pet. Chem.* **2019**, *59*, 1269–1277. [[CrossRef](#)]
3. Sviridenko, N.N.; Golovko, A.K.; Kirik, N.P.; Anshits, A.G. Upgrading of heavy crude oil by thermal and catalytic cracking in the presence of NiCr/WC catalyst. *J. Taiwan Inst. Chem. Eng.* **2020**, *112*, 97–105. [[CrossRef](#)]
4. Al-Attas, T.; Ali, S.A.; Zahir, M.H.; Xiong, Q.; Al-Bogami, S.A.; Malaibari, Z.O.; Razzak, S.A.; Hossain, M.M. Recent Advances in Heavy Oil Upgrading using Dispersed Catalysts. *Energy Fuels* **2019**, *33*, 7917–7949. [[CrossRef](#)]
5. Nguyen, N.T.; Kang, K.H.; Pham, H.H.; Go, K.S.; Pham, D.V.; Seo, P.W.; Nho, N.S.; Lee, C.W.; Park, S. Catalytic hydrocracking of vacuum residue in a semi-batch reactor: Effect of catalyst concentration on asphaltene conversion and product distribution. *J. Ind. Eng. Chem.* **2021**, *102*, 112–121. [[CrossRef](#)]
6. Ajumobi, O.O.; Muraza, O.; Kondoh, H.; Hasegawa, N.; Nakasaka, Y.; Yoshikawa, T.; Al Amer, A.M.; Masuda, T. Upgrading oil sand bitumen under superheated steam over ceria-based nanocomposite catalysts. *Appl. Energy* **2018**, *218*, 1–9. [[CrossRef](#)]
7. Kim, S.H.; Kim, K.D.; Lee, Y.K. Effects of dispersed MoS<sub>2</sub> catalysts and reaction conditions on slurry phase hydrocracking of vacuum residue. *J. Catal.* **2017**, *347*, 127–137. [[CrossRef](#)]
8. Gray, M.R. Upgrading petroleum residues and heavy oils. *Fuel Energy Abstr.* **1994**, *4*, 348.
9. Sreedhara, S.; Huh, K.Y.; Park, H. Numerical investigation for combustion characteristics of vacuum residue (VR) in a test furnace. *Energy* **2007**, *32*, 1690–1697. [[CrossRef](#)]
10. Ichinose, T.; Fujimura, K.; Takeno, K.; Motai, T.; Arakawa, Y.; Fujii, H. Combustion characteristics and pollution minimum technology for VR (vacuum residue) fired boiler. *JSME Int. J.* **1998**, *41*, 1055–1060. [[CrossRef](#)]
11. Fujimura, K.; Mastumoto, H.; Arakawa, Y.; Fujii, H.; Mizoguchi, T. Development and Operation Results of VR Firing Boiler. *Mitsubishi Juko Gih.* **1999**, *36*, 96–99.
12. Park, H.Y.; Kim, T.H. Non-isothermal pyrolysis of vacuum residue (VR) in a thermogravimetric analyzer. *Energy Convers. Manag.* **2006**, *47*, 2118–2127. [[CrossRef](#)]
13. Goncharov, A.V.; Krivtsov, E.B. Calculation of the rate constants of thermal cracking and condensation reactions of high-sulfur tar asphaltenes. *Solid Fuel Chem.* **2022**, *56*, 108–115. [[CrossRef](#)]
14. Nguyen, N.T.; Park, S.; Jung, J.; Cho, J.; Lee, C.W.; Park, Y.-K. Comparative reactivity between thermal and catalytic hydrocracking of vacuum residue: Effect of asphaltenes. *J. Ind. Eng. Chem.* **2018**, *61*, 32–38. [[CrossRef](#)]
15. Shi, Q.; Zhao, S.; Zhou, Y.; Gao, J.; Xu, C. Development of heavy oil upgrading technologies in China. *Rev. Chem. Eng.* **2019**, *36*, 19. [[CrossRef](#)]
16. Zhao, Y.; Xu, C.; Zhao, S.; Shi, Q. Pattern Recognition Technology Application in Intelligent Processing of Heavy Oil. *Energy Fuels* **2012**, *26*, 7251–7256. [[CrossRef](#)]
17. Stratiev, D.; Shishkova, I.; Tankov, I.; Pavlova, A. Challenges in characterization of residual oils. A review. *J. Pet. Sci. Eng.* **2019**, *178*, 227–250. [[CrossRef](#)]
18. Strelets, L.A.; Ilyin, S.O. Effect of enhanced oil recovery on the composition and rheological properties of heavy crude oil. *J. Pet. Sci. Eng.* **2021**, *203*, 108641. [[CrossRef](#)]

19. Haktanır, M.; Karahan, S.; Yaşar, M. Structurally explicit composition model of petroleum vacuum residue. *Fuel* **2021**, *300*, 120977. [[CrossRef](#)]
20. Bradley, L.C.; Miller, S.F.; Miller, B.G.; Tillman, D.A. A Study on the Relationship between Fuel Composition and Pyrolysis Kinetics. *Energy Fuels* **2011**, *25*, 1989–1995. [[CrossRef](#)]
21. Vyazovkin, S.; Burnham, A.K.; Criado, J.M.; Pérez-Maqueda, L.A.; Popescu, C.; Sbirrazzuoli, N. ICTAC Kinetics Committee recommendations for performing kinetic computations on thermal analysis data. *Thermochim. Acta* **2011**, *520*, 1–19. [[CrossRef](#)]
22. Vyazovkin, S.; Wight, C.A. Model-free and model-fitting approaches to kinetic analysis of isothermal and nonisothermal data. *Thermochim. Acta* **1999**, *340*, 53–68. [[CrossRef](#)]
23. Flynn, J.H. The “Temperature Integral”—Its use and abuse. *Thermochim. Acta* **1997**, *300*, 83–92. [[CrossRef](#)]
24. Nguyen-Huy, C.; Shin, E.W. Hierarchical macro–mesoporous Al<sub>2</sub>O<sub>3</sub>-supported NiK catalyst for steam catalytic cracking of vacuum residue. *Fuel* **2016**, *169*, 1–6. [[CrossRef](#)]
25. Hosseinpour, M.; Fatemi, S.; Ahmadi, S.J. Catalytic cracking of petroleum vacuum residue in supercritical water media: Impact of  $\alpha$ -Fe<sub>2</sub>O<sub>3</sub> in the form of free nanoparticles and silica-supported granules. *Fuel* **2015**, *159*, 538–549. [[CrossRef](#)]
26. Gao, H.; Wang, G.; Wang, H.; Chen, J.; Xu, C.; Gao, J. A Conceptual Catalytic Cracking Process to Treat Vacuum Residue and Vacuum Gas Oil in Different Reactors. *Energy Fuels* **2012**, *26*, 1870–1879. [[CrossRef](#)]
27. Li, Q.; Xiao, Z.; Xin, H.; Li, G.; Wang, D.; Feng, C.; Li, X.; Chen, S.; Chung, K.H. Enhancement of hydrotreating activity of oil-soluble CoMo<sub>6</sub> heteropolyacid for 4, 6-dimethyldibenzothiophene and vacuum residue by controlling sulfurization degree. *Chem. Eng. J.* **2023**, *472*, 145128. [[CrossRef](#)]
28. Lee, H.S.; Nguyen-Huy, C.; Pham, T.-T.; Shin, E.W. ZrO<sub>2</sub>-impregnated red mud as a novel catalyst for steam catalytic cracking of vacuum residue. *Fuel* **2016**, *165*, 462–467. [[CrossRef](#)]
29. Nguyen-Huy, C.; Shin, E.W. Amelioration of catalytic activity in steam catalytic cracking of vacuum residue with ZrO<sub>2</sub>-impregnated macro–mesoporous red mud. *Fuel* **2016**, *179*, 17–24. [[CrossRef](#)]
30. Che, Y.; Yuan, M.; Qiao, Y.; Liu, Q.; Zhang, J.; Tian, Y. Fundamental study of hierarchical millisecond gas-phase catalytic cracking process for enhancing the production of light olefins from vacuum residue. *Fuel* **2019**, *237*, 1–9. [[CrossRef](#)]
31. Che, Y.; Yang, Z.; Qiao, Y.; Tian, Y. Study on catalytic pyrolysis of vacuum residue and its eight group-fractions with solid acid-base mixed catalysts by Py-GC/MS. *Fuel Process. Technol.* **2019**, *188*, 22–29. [[CrossRef](#)]
32. Lourenço, M.P.; de Oliveira, C.; Oliveira, A.F.; Guimaraes, L.; Duarte, H.A. Structural, Electronic, and Mechanical Properties of Single-Walled Chrysotile Nanotube Models. *J. Phys. Chem.* **2012**, *116*, 9405–9411. [[CrossRef](#)]
33. Cao, X.; Chuan, X.Y.; Huang, D.B. Structure performance and application research of natural nano-tubular chrysotile. *J. Funct. Mater.* **2013**, *14*, 1984–1989. [[CrossRef](#)]
34. Pyrzynska, K. Carbon nanostructures for separation, preconcentration and speciation of metal ions. *TrAC Trends Anal. Chem.* **2010**, *29*, 718–727. [[CrossRef](#)]
35. Tan, X.; Fang, M.; Chen, C.; Yu, S.; Wang, X. Counterion effects of nickel and sodium dodecylbenzene sulfonate adsorption to multiwalled carbon nanotubes in aqueous solution. *Carbon* **2008**, *46*, 1741–1750. [[CrossRef](#)]
36. Balpanova, N.Z.; Baikenov, M.I.; Gyulmaliev, A.M.; Absat, Z.B.; Batkhan, Z.; Ma, F.; Su, K.; Kim, S.V.; Baikenova, G.G.; Aitbekova, D.E.; et al. Thermokinetic parameters of the primary coal tars destruction in the presence of catalysts and polymeric materials. *Bull. Univ. Karaganda. Ser. Chem.* **2021**, *2*, 86–95. [[CrossRef](#)]
37. Strizhakov, D.A.; Yusevich, A.I.; Yurachka, V.V.; Kadiev, K.M.; Agabekov, V.E.; Khadzhiev, S.N. Kinetics of thermolysis of vacuum tower bottoms mixed with pine sawdust. *Pet. Chem.* **2016**, *56*, 703–710. [[CrossRef](#)]
38. Kök, M.V. Non-isothermal kinetic analysis and feasibility study of medium grade crude oil field. *J. Therm. Anal. Calorim.* **2008**, *91*, 745–748. [[CrossRef](#)]
39. Ozawa, T. Kinetic analysis of derivative curves in thermal analysis. *J. Therm. Anal.* **1970**, *2*, 301–324. [[CrossRef](#)]
40. Doyle, C.D. Kinetic analysis of thermogravimetric data. *Appl. Polym. Sci.* **1961**, *15*, 285. [[CrossRef](#)]
41. Che, Y.; Yang, Z.; Qiao, Y.; Zhang, J.; Tian, Y. Study on pyrolysis characteristics and kinetics of vacuum residue and its eight group-fractions by TG-FTIR. *Thermochim. Acta.* **2018**, *669*, 149–155. [[CrossRef](#)]
42. Tyanakh, S.; Murzabek, B.; Tusipkhan, A.; Aitbekova, D.; Balpanova, N.; Ma, F.Y. Kinetic Study of the Thermolysis Process of Oil Sludge (Atasualashankou) With Nickel, Cobalt and Iron Deposited on Microsilicate. *East. Eur. J. Enterp. Technol.* **2022**, *2*, 19–24.

**Disclaimer/Publisher’s Note:** The statements, opinions and data contained in all publications are solely those of the individual author(s) and contributor(s) and not of MDPI and/or the editor(s). MDPI and/or the editor(s) disclaim responsibility for any injury to people or property resulting from any ideas, methods, instructions or products referred to in the content.